



Study on the influence of armature on the efficiency of reluctance accelerator

Hui-min Deng, Yu Wang, Zhong-ming Yan*

School of Electrical Engineering, Southwest Jiaotong University, Chengdu, 610031, China

ARTICLE INFO

Article history:

Received 24 October 2020

Received in revised form

8 January 2021

Accepted 18 January 2021

Available online xxx

Keywords:

Reluctance accelerator

Armature design

Soft magnetic material

Magnetic force calculation

Energy transformation efficiency

ABSTRACT

The armature is an important part affecting the energy conversion efficiency of a reluctance accelerator. In this paper, six kinds of soft magnetic materials are chosen and four structures are designed for the armature. At first, the circuit and magnetic force are theoretically analyzed. Then the armatures with different materials and structures are used in the simulation, and the performances are compared and analyzed. At last, the experiment verifies the theory analysis and simulation design. It is concluded that the saturation flux density and conductivity of the material are the key factors affecting the armature force, and the optimization of armature structure can effectively restrain the eddy current, reduce negative force and improve efficiency. Compared with cutting slits in solid armatures, laminating the sheets radially can reduce the eddy current more efficiently. Although slitting can prevent the eddy current to a certain extent, meanwhile, it will decrease the magnetic force because of the losing of magnetized volume and the surface area. Hence, choosing the high saturation flux density material and making out the armature with radially_laminated sheets will improve the efficiency of the reluctance accelerator. In this paper, the silicon steel radially_laminated armature is a better choice for the armature design of the reluctance accelerator.

© 2021 China Ordnance Society. Production and hosting by Elsevier B.V. on behalf of KeAi Communications Co. This is an open access article under the CC BY-NC-ND license (<http://creativecommons.org/licenses/by-nc-nd/4.0/>).

1. Introduction

Compared with railgun, coilgun has the advantages of low wear of the system and long operational lifetime due to no physical contact with the armature [1–3]. Coilgun is mainly divided into induction type and reluctance type. Reluctance-type coilgun is also called reluctance accelerator that requires lower current than induction-type to generate appreciable acceleration for the armature, which simplifies the switching circuit, but still exhibits relatively good efficiency than induction-type [2,4,5]. The armature used in this accelerator is even smaller [6]. The reluctance accelerator has another advantage that can maintain structural reliability and robust performance in hostile environment [2,4]. By contrary, the induced eddy current in the armature of induction coilgun will generate a large amount of heat which will lead to degradation in its performance and controllability [2]. Therefore,

the reluctance accelerator is suitable to be used in the circumstances of low power, simple drive circuit and high requirement for heat dissipation rather than an induction coilgun. Reluctance accelerator can not only be used as a coil gun to accelerate projectiles, but also has been used as a variety of actuators and electromagnetic tools for industrial machinery (e.g a linear reluctance self-oscillating motor for the driving shuttle of a weaving loom or the pneumatic hammer, a reluctance shuttle device, nail-guns, pumps for electrochemists, and many other electromechanical systems) [7–11].

Reluctance accelerator is a device that transforms the electromagnetic energy to mechanical energy, and the conversion efficiency is worthy of discussion. In recent years, many studies have been done to increase its efficiency [2,3,12–25]. The armature plays an important role in affecting the energy conversion efficiency of the reluctance accelerator. The armature of reluctance accelerator is ferromagnetic material, which can be conductive or non-conductive. It can be seen from a lot of research that choosing a suitable armature material is crucial for the optimization of the reluctance accelerator. Slade [7] developed a simplified field-based physical model from basic principles and cast in a variational

* Corresponding author.

E-mail addresses: dhm3611@163.com (H.-m. Deng), wangyu@swjtu.edu.cn (Y. Wang), yzm@swjtu.edu.cn (Z.-m. Yan).

Peer review under responsibility of China Ordnance Society

(Lagrangian) form. From the mathematical model, it can be concluded that using an armature with a high saturation flux density is beneficial for improving the energy transfer efficiency, but the initial permeability is not so crucial for that. Slade done simulation and experiment comparison with ferrite and mild steel to verify the effect of saturation flux density of the armature material in his paper. The efficiency reached approximately 9% by using mild steel armature in Slade's research. But the eddy current was ignored in his research, so there was no analysis on conductivity of the armature in theory model and experiment. Although several methods were put forward to minimize the eddy current in armature, there were no theory, simulation and experiment to support these ideas. Barrera [12] chose three magnetic materials to analyze and compared the effects on energy transfer efficiency of different saturation values. Meanwhile, the method of cutting slits in the armature can reduce the eddy current is verified by experiment in this paper. The maximum efficiency in Barrera's study is 8.53%. However, the mathematical model used in Barrera's work was that of Slade's, so there was no physical explanation how the conductivity affect the efficiency in the theory. DALDABAN [13] used AISI1020 and AISI1050 projectiles to compare their performances, and AISI1050 gained a higher muzzle velocity because of its higher permeability. The accelerator of DALDABAN designed gained the efficiency of 2.04% by using three stages. But there was lack of theory analysis and the two materials belongs to one kind of soft magnetic material. The samples are too few, and the comparison result was not significant. Xiang [14] proposed and compared the armatures with three different structures with one kind material to analyze the efficiency and firing accuracy of reluctance accelerator. The maxim efficiency is 2.87% for cylindrical armature with notch. It only proved that slitting can reduce eddy currents. There was also lack of theory analysis and material comparison. The works [15,16] also studied effects of the magnetic material and structure to the energy transfer efficiency. The highest efficiency value (3.01%) is obtained in the with the 8-cm 1050 projectile [16]. Lack of enough kinds of material still existed in these studies. Overall, there are some problems in the previous research. The types of armatures were not enough and systematic; the properties of magnetic material was not elaborated or expounded too little; the theory analysis did not involve the influence of the conductivity to the force exerted on the armature; the method to weaken the eddy current in the armature is single, so there was no comparison analysis in the methods. In addition, the factors of armature influencing the efficiency were not comparatively analyzed and not summarized together in only one research. Most of the efficiencies in these studies were below 4%. Only minority were approximately 9% by using a field-concentrating sheath which can increase the efficiency [26].

To choose suitable armature material and structure to improve the energy conversion efficiency, we systematically and comprehensively compare, analyze and summarize the influence of armature on the efficiency of reluctance accelerator. Firstly, the force exerted on the armature is analyzed theoretically, and various factors of the influencing the magnetic force on the armature is studied on the basis of the physical essence. Especially, the calculation of volume force density and the effect of conductivity of the armature on the force are elaborated in detail. Secondly, armatures with six kinds of soft magnetic material and four kinds of structures are chosen, and the impact of the various factors on efficiency is analyzed and compared, and the factors include conductivity, saturation flux density and structure. Through the use of more comprehensive structures and materials than ever before for centralized comparison, this work not only verifies the conclusion of the previous researches by simulation and experiment, but also provides a clearer reference for selecting a suitable armature and

improving the energy conversion efficiency. In this paper, the armature made out of radially-laminated silicon steel sheets achieves the most efficiency, and this type of armature has never been designed for the reluctance accelerator in previous researches. The study on the armature can also provide references for the design of other electromagnetic devices using ferromagnetic materials.

2. Theoretical analysis

2.1. Circuit analysis

The model of the reluctance accelerator is shown in Fig. 1. The accelerator consists of a drive coil, a tube and a ferromagnetic armature. When the drive coil is energized by the power, the armature is magnetized by the magnetic field. The electromagnetic attraction force will pull the armature into the coil. If the drive coil still has current when the armature passes the middle of the coil, a reverse force will be generated and reduce the speed and suck the projectile back, which is called suck-back effect. So the current must be cut off as soon as possible when the centerlines of the projectile and the drive coils is about to overlap.

An improved discharging circuit is opted as the drive circuit of the reluctance accelerator, which prevents the suck-back effect and increases the efficiency [17], as shown in Fig. 2. The whole discharging process contains three steps. The first step, the thyristor THY1 is off and IGBT1 is on, and the drive coil is energized by the capacitor bank. The circuit is modeled as RLC circuit, and Kirchhof's voltage law is written as

$$\frac{dL(x)i(t)}{dt} + Ri(t) - u(t) = 0. \quad (1)$$

$$\frac{dL(x)i(t)}{dt} = L(x) \cdot \frac{di(t)}{dt} + i(t) \cdot \frac{dL(x)}{dx} \cdot \frac{dx}{dt} \quad (2)$$

$$i(t) = -C \frac{du(t)}{dt} \quad (3)$$

$$C \left(L(x) \frac{d^2u(t)}{dt^2} + \frac{dL(x)}{dx} \cdot \frac{dx}{dt} \cdot \frac{du(t)}{dt} \right) + RC \frac{du(t)}{dt} = -u(t) \quad (4)$$

where $L(x)$ is the inductance of drive coil, which is a quantity related to the position of armature. C is the capacitance of the capacitor bank for discharging. R is the resistor of the circuit, $u(t)$ is the voltage of the capacitor bank, and $i(t)$ is the current in coil.

At the second step, the current will flow through D1 as soon as the voltage of capacitor decreases to zero, and the current in the coil decays according to the exponential law. The electric equation in this RL circuit can be expressed as

$$L(x) \frac{di(t)}{dt} + i(t) \frac{dL(x)}{dx} \cdot \frac{dx}{dt} + Ri(t) = 0 \quad (5)$$

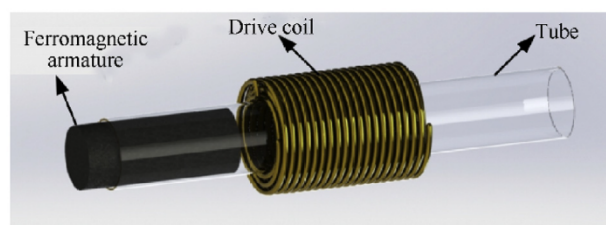


Fig. 1. The model of the reluctance accelerator.

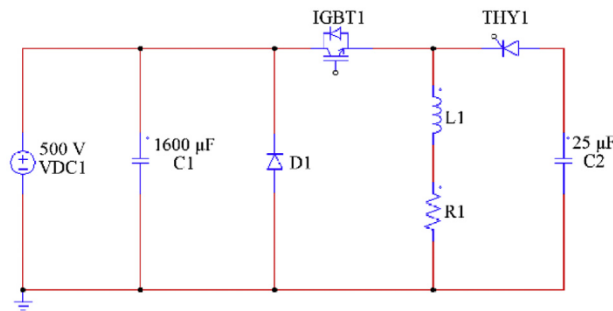


Fig. 2. Drive circuit schematic diagram.

At the last step, IGBT1 is turned off and THY1 is switched on when the armature is getting to the center of the coil. The current flows through C2 and charges it. The residual voltage direction of C2 is opposite to that of the initial charging voltage. The circuit in the last step of the discharging process can also be solved by Eq. (4). But the C and $u(t)$ are referred to the capacitance and the voltage of C2, respectively.

2.2. Transient diffusion equations

The pulsed magnetic field is quasi-stationary, so the displacement current can be neglected. The Maxwell's equations in this problem can be written as:

$$\nabla \times \mathbf{H} = \mathbf{J} \quad (6)$$

$$\nabla \times \mathbf{E} = -\frac{\partial \mathbf{B}}{\partial t} \quad (7)$$

$$\nabla \cdot \mathbf{B} = 0 \quad (8)$$

And the constitutive equations are:

$$\mathbf{B} = \mu \mathbf{H} \quad (9)$$

$$\mathbf{J} = \sigma \mathbf{E} \quad (10)$$

where \mathbf{H} is the magnetic field intensity, \mathbf{B} is the magnetic induction, \mathbf{E} is the electric field intensity, \mathbf{J} is the current density, μ is the permeability, which is a function of \mathbf{H} , can be written as $\mu(H)$, σ is the conductivity.

The divergence of a curl is always zero, according to Eq (8), the magnetic induction \mathbf{B} can be expressed as the curl of magnetic vector potential \mathbf{A} :

$$\mathbf{B} = \nabla \times \mathbf{A} \quad (11)$$

The solution domain of the reluctance accelerator includes three regions, which are air, drive coil and armature respectively, as shown in Fig. 3. The diffusion equations may be specialized to the varied parts as follows [27]: for the source free air region,

$$\frac{1}{\mu_0} \nabla \times \nabla \times \mathbf{A} = 0 \quad (12)$$

for the linear source region, drive coil part,

$$\frac{1}{\mu_0} \nabla \times \nabla \times \mathbf{A} = \mathbf{J}_s \quad (13)$$

for the source free nonlinear eddy current and movable armature

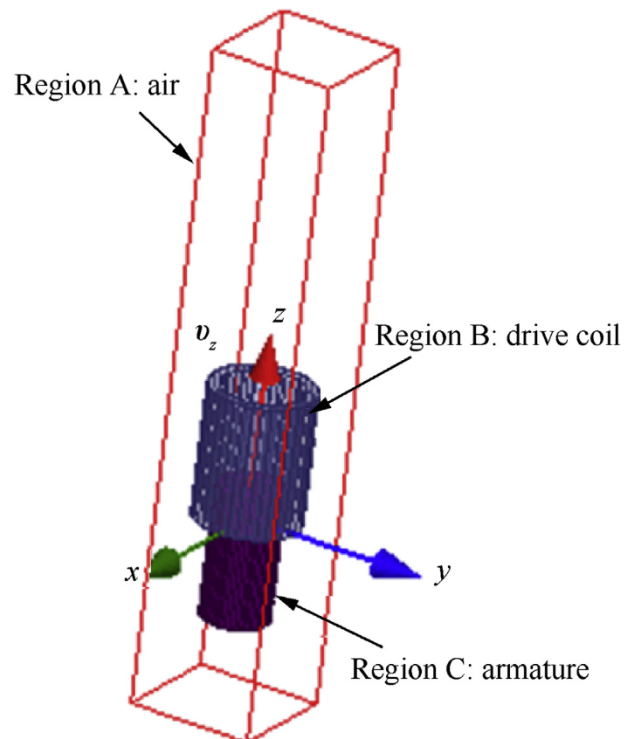


Fig. 3. Solution domain of the reluctance accelerator.

region,

$$\nabla \times \left(\frac{1}{\mu} \nabla \times \mathbf{A} \right) = \mathbf{J}_f = \sigma \left(-\frac{\partial \mathbf{A}}{\partial t} - \mathbf{v} \times (\nabla \times \mathbf{A}) \right) \quad (14)$$

where μ_0 is the permeability of air, \mathbf{J}_s is the excitation current density in the coil, \mathbf{J}_f is the induced eddy current in the armature, \mathbf{v} is the velocity of the armature.

2.3. B–H curves interproximation

B–H Curves, which describe the nonlinear relation between the magnetic induction \mathbf{B} and the magnetic field intensity \mathbf{H} , are used to model ferromagnetic materials in connection with electromagnetic field computation. In our problem, the soft magnetic materials are isotropic, and the hysteresis is neglected. B–H curves are generally established by giving tabulated sets of B–H values which obtained by experimental measurements on ferromagnetic materials. The B–H curves of soft magnetic material are modeled to be single valued in our problem. For computer implementation, it is desirable to model the B–H curve by an appropriate mathematical expression or by suitable numerical method. Interpolation method is generally used to approximate the curve [28,29]. The Akima's interpolation method provides a natural and more suitable procedure for the smooth curve fitting of experimental data [30,31]. The approximate B–H curve obtained by this method is monotony, smooth and does not appear unwanted jitter. According to the Akima's interpolation method, for a set of data points

$$B_i = B(H_i), \quad 1 \leq i \leq k \quad (15)$$

The interpolation function can be defined as

$$B(H) = a_0 + a_1(H - H_i) + a_2(H - H_i)^2 + a_3(H - H_i)^3$$

$$H_i \leq H \leq H_{i+1} \quad (16)$$

To determine the coefficients a_0 , a_1 , a_2 and a_3 of the interpolation polynomial for each interval $[H_i, H_{i+1}]$, the function values B_i and B_{i+1} , and the first derivatives B'_i and B'_{i+1} at the end points of the interval are used. The first derivative B'_i of the interpolation function at H_i is estimated from the data for this point and the next two points on each side of H_i . Using the ratios

$$m_j = \frac{B_{j+1} - B_j}{H_{j+1} - H_j}, \quad j = i-2, i-1, i, i+1 \quad (17)$$

the estimated derivative B'_i is defined as

$$B'_i = \frac{|m_{i+1} - m_i|m_{i-1} + |m_{i-1} - m_{i-2}|m_i}{|m_{i+1} - m_i| + |m_{i-1} - m_{i-2}|} \quad (18)$$

Several special cases for B'_i have to be considered.

$$B'_i = \begin{cases} m_{i-1}, m_{i-2} = m_{i-1} \wedge m_i \neq m_{i+1} \\ m_i, m_i = m_{i+1} \wedge m_{i-2} \neq m_{i-1} \\ m_{i-1} = m_i, m_{i-1} = m_i \\ \frac{m_{i-1} - m_i}{2}, m_{i-2} = m_{i-1} \neq m_i = m_{i+1} \end{cases} \quad (19)$$

At the end of the curve, two more points have to be estimated based on the given points. The order of the interpolation function reduces to 2 for these intervals, the function can be written as

$$B(H) = b_0 + b_1(H - H_i) + b_2(H - H_i)^2 \quad (20)$$

To be able to use Eq. (18) for calculating the derivatives B'_1 , B'_2 , B'_{k-1} and B'_k additional ratios m_{-1} , m_0 , m_k , and m_{k+1} have to be estimated.

$$m_{-1} = 2m_0 - m_1 \quad (21)$$

$$m_0 = 2m_1 - m_2 \quad (22)$$

$$m_k = 2m_{k-1} - m_{k-2} \quad (23)$$

$$m_{k+1} = 2m_k - m_{k-1} \quad (24)$$

2.4. Electromagnetic force calculation

The calculation of the magnetic force acting on the current carrying conductor and ferromagnetic objects is of great importance for designing the electric-magnetic energy transformation device, which is the foundation to predict the performance of the device. The force calculation is an important topic in the domain of the numerical computation of electromagnetic fields. The calculation methods of electromagnetic force exerted on armatures were discussed and analyzed comprehensively in many previous literatures [32–47]. There are a number of different methods to calculate the magnetic force.

In general, these methods can be classified into two groups. The first group contains the Maxwell stress tensor method and virtual-work principle method. They are used to calculate total force of the objects in the magnetic field. They have more a mathematical than physical meaning. The second group contains the equivalent source methods (equivalent charge or current) and the methods based on Lorentz formula. Some of the time, we need to calculate the local

force, and want to understand the physical meaning of the force and the influencing factors, so the second group of calculation methods is appropriate.

According to electromagnetic theory, the force of magnetic field on current carrying conductor and ferromagnetic object is transmitted through medium. There is stress in magnetic medium (vacuum or air), that is, the tension along the magnetic line of force and the direction perpendicular to the magnetic line of force. If we select a closed surface lying in the air to enclose the armature of interest, the electromagnetic stress acting on any unit surface area in vacuum medium is

$$\mathbf{f}_{\text{mst}} = \frac{1}{\mu_0} (\mathbf{n} \cdot \mathbf{B}_{\text{air}}) \mathbf{B}_{\text{air}} - \frac{1}{2\mu_0} \mathbf{B}_{\text{air}}^2 \mathbf{n} \quad (25)$$

where \mathbf{f}_{mst} denotes the surface force density, \mathbf{B}_{air} the magnetic induction on the air side, \mathbf{n} is a unit vector normal to the surface element. This method is called Maxwell stress tensor. The surface density of the force in the normal direction is:

$$f_n = \frac{\mu_2 - \mu_1}{2\mu_1\mu_2} \left(B_{1n}^2 + \frac{\mu_2}{\mu_1} B_{1t}^2 \right) \quad (26)$$

where μ_1 and μ_2 denotes the permeability of air and magnetic material, B_{1n} and B_{1t} represent the normal and tangential component of magnetic induction on the air side.

Maxwell stress tensor and Virtual-work principle are closely related. Virtual work principle is an alternative method for the former one. When the B–H relationship is nonlinear, the magnetic energy and force is:

$$W = \int_V \left(\int_0^B \mathbf{H} \cdot d\mathbf{B} \right) dV \quad (27)$$

$$F = - \frac{\partial W}{\partial s} \quad (28)$$

The armature of the reluctance accelerator is ferromagnetic material, which may or may not be conductive. According to the theory of electrodynamics, electromagnetic material in the transient electromagnetic field is exerted not only by the magnetic force caused by the magnetization but also by the Lorentz force caused by the induced current in the conductor. When the pulsed current flows through the drive coil, the eddy current is simultaneously induced in the conductive armature. The volume magnetic force density on the armature can be expressed by the resultant force of two parts of forces. To analyze the local force volume density, the second group of methods is needed. They are magnetic charge method, magnetizing current method, Kelvin force density method, Korteweg–Helmholtz force density method, etc. The volume force density calculation methods are listed in Table 1 where J_f is eddy current density in armature, J_m is the magnetizing current density, \mathbf{B} is magnetic flux density, M is the magnetization, μ is permeability of the armature, α_i represents material properties, such as density and magnetic permeability that varies with position. In our problem, α_i stands for magnetic permeability. The first term in these equations in Table 1 stands for the Lorentz force density, which denotes the force per unit volume on a current-carrying conductor in a magnetic field, marked as \mathbf{f}_L . The second term is the magnetization force density, marked as \mathbf{f}_M . The resultant force applied on the armature is the sum of the two kinds of force. If the ferromagnetic material is nonconductive, the first term can be neglected.

When the projectile enters the coil, the Lorentz force and the

Table 1

Methods of calculation of volume force density.

$$\mathbf{B} = \mu_0(\mathbf{H} + \mathbf{M}) \quad (29)$$

$$\mathbf{J}_m = \nabla \times \mathbf{M} \quad (30)$$

| Methods | Volume force density equations |
|----------------------------------|---|
| Magnetizing current density | $\mathbf{f} = \mathbf{J}_f \times \mathbf{B} + \mathbf{J}_m \times \mathbf{B}$ |
| Magnetic charge density | $\mathbf{f} = \mathbf{J}_f \times \mathbf{B} - \mu_0 \mathbf{H} \nabla \cdot \mathbf{M}$ |
| Korteweg-Helmholtz force density | $\mathbf{f} = \mathbf{J}_f \times \mathbf{B} + \sum_i \frac{\partial W}{\partial \alpha_i} \nabla \alpha_i$ |
| Kelvin force density | $\mathbf{f} = \mathbf{J}_f \times \mathbf{B} + \mu_0 \mathbf{M} \cdot \nabla \mathbf{H}$ |

magnetization force are repulsive and attractive respectively. For our problem, Lorentz force will decrease the speed of the armature and reduce the efficiency of the energy conversion. According to Eq. (10), eddy current density in the armature is proportional to conductivity. Hence, to choose a low conductive material or to optimize the construction of the armature to reduce the eddy current density can improve the armature performance. So this equation provides reference to choose and design the armature.

To calculate the field values, the boundary conditions must be satisfied on the interfaces between different media [42].

$$\nabla \cdot \mathbf{B} = 0 \text{ or } B_{1n} = B_{2n} \quad (31)$$

$$\nabla \times \mathbf{H} = 0, \text{ or } H_{1t} = H_{2t} \quad (32)$$

When there is no field source on the boundary.

2.5. Kinematic equations

For the reluctance accelerator moving system, only the axial motion is concerned, and only the longitudinal force needs to be calculated. The kinematic equations of the armature are written as:

$$F = m_a \frac{dv_z}{dt} \quad (33)$$

$$\frac{dz}{dt} = v_z \quad (34)$$

where m_a is the mass of the armature, v_z is the z-directed (axial) velocity, and z is the position of the armature respect to the start point. The energy transformation efficiency of the reluctance accelerator can be expressed as

$$\rho = \frac{m_a v_0^2}{C_1 U_0^2 - C_2 U_c^2} \quad (35)$$

where C_1 is the capacitance of C_1 in Fig. 2, U_0 is the initial voltage of C_1 , C_2 is the capacitance of C_2 in Fig. 2, U_c is the charging voltage of C_2 . v_0 is the muzzle velocity of the armature.

3. Simulation analysis

To simulate the motion of the accelerator, the finite element method (FEM) simulation software ANSYS Maxwell is utilized. In this section, the simulation model is described; the results and performances of different armature are compared and analyzed.

Table 2

Transient simulation model dimensions.

| | | |
|------------|----------------------------------|---------|
| Drive coil | Material | Copper |
| | Number of turns | 140 |
| | Length | 60 mm |
| | Thickness | 5 mm |
| | Inner radius | 18.5 mm |
| Armatures | Airgap between coil and armature | 3.5 mm |
| | Radius | 15 mm |
| | Length | 60 mm |

3.1. Simulation model

Due to the special structure of the armature, 3-D simulation model is used and shown in Fig. 3. Table 2 exhibits the dimensions of the simulation model. In order to design an armature which can improve the efficiency of the reluctance accelerator, the influences of material and structure must be analyzed.

3.1.1. Material

Six kinds of soft magnetic materials are chosen here, which almost cover the kinds commonly used in motors. They are silicon steel sheet (20JNEH1200), iron (DT4C), iron-colbalt alloy (1J27), amorphous alloy (1K101), permalloy (1J50), and ferrite (PC40). The basic electromagnetic properties of these materials are listed in Table 3. B_s represents the saturation flux density. The B–H curves and μ -H curves of these materials are shown in Fig. 4.

3.1.2. Structure

Based on the electric property of the soft magnetic materials and the theory analysis above, the conductive armatures will be exerted by the Lorentz force caused by the eddy current, and the energy conversion efficiency will be lowered down by this negative force. In order to reduce the Lorentz force, some measures have to be taken to restrain the eddy current. Therefore, four kinds of structures are designed here to compare. The details of the classification of armature structures are shown in Table 4.

The six materials are divided into two groups according to the manufacture form. One group is the form of rod, the other is the form of sheet. For the form of rod, we choose four different materials, all of which are processed into solid cylinder, which is the basic structure without modification. Besides ferrite armature (conductivity can be ignored), materials with obvious conductivity are cut with 8 slits from the edge to the center around the solid cylinder. The width of the slit is 1 mm, and the depth is 12 mm. As a measure to reduce eddy current, slitting is used to compare with the solid cylinder structure.

For the form of sheet, we choose two materials of silicon steel and amorphous alloy. They are both radially laminated to break the paths which eddy currents can flow through, because the sheets are insulated from each other. Meanwhile, the silicon steel sheets are also axially laminated, the purpose of which is to compare with the radially lamination structure. Although the axially_lamination cannot prevent the formation of eddy current, this structure can reduce the eddy current density of the whole armature because of the insulating material on the sheet. There are not only comparisons of different materials based on the same structure but also comparisons of different structures based on the same material in this study.

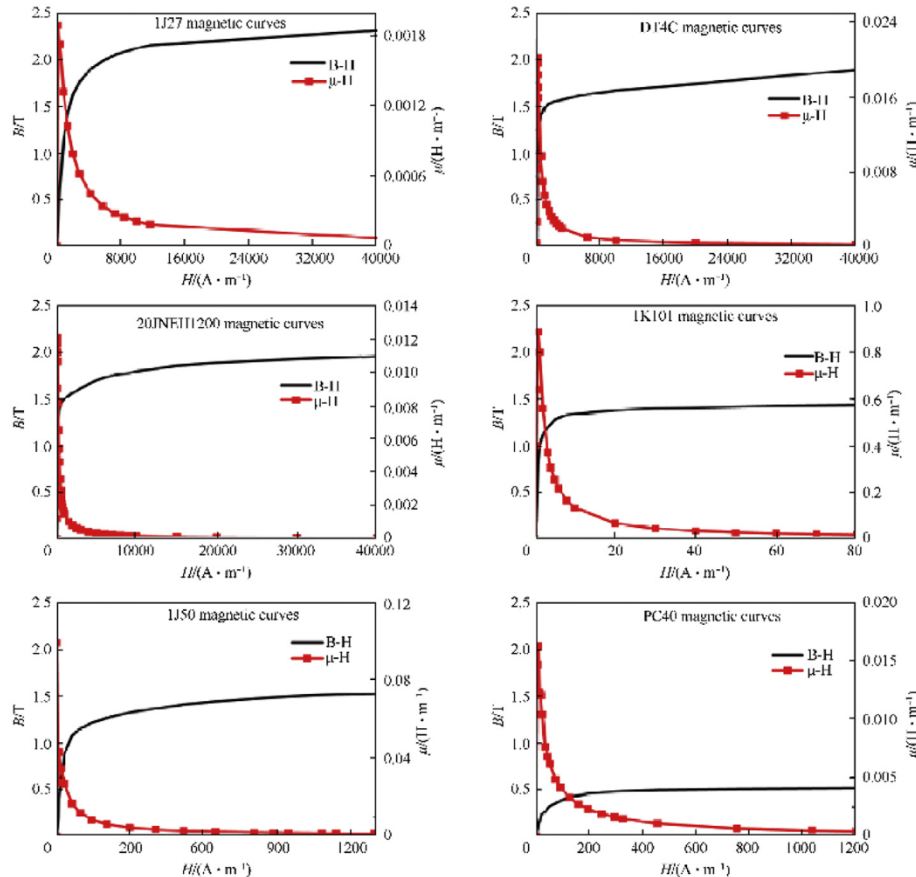
3.1.3. Other simulation parameters

The initial position, which is the distance from the centerline of drive coil to the front-end of the armature will affect the performance of the accelerator, and an optimal position can make the armature gain the maximum kinetic energy [24,25]. Comparing the

Table 3

Electromagnetic properties of materials of armature.

| Parameters | Material | | | | | |
|--|--------------------------|----------------------|----------------------------------|-------------------------|----------------------|----------------|
| | Iron-colbat alloy (1J27) | Iron (DT4C) | Silicon Steel sheet (20JNEH1200) | Amorphous alloy (1K101) | Permalloy (1J50) | Ferrite (PC40) |
| B_s/T | 2.36 | 2.2 | 2.03 | 1.56 | 1.50 | 0.51 |
| Conductivity/(Simens·m ⁻¹) | 5.26*10 ⁶ | 9.09*10 ⁶ | 1.81*10 ⁶ | 7.69*10 ⁵ | 2.22*10 ⁶ | 0.15 |

**Fig. 4.** The B–H curves and μ -H curves of different materials.**Table 4**

Classifications of the armature structure.

| Form | Rod | Sheet | | |
|-----------|------------------------------|---------------------------|-------------------------------|------------------------------|
| Material | 1J27 DT4C 1J50 PC40 | 1J27 DT4C 1J50 | 20JNEH1200 1K101 | 20JNEH1200 |
| Structure | Solid cylinder | Cylinder with 8 slits | Radially-laminated sheets | Axially-laminated sheets |

Table 5

Simulated results of different Armatures.

| Material | Structure | Mass/g | Velocity/(m·s ⁻¹) | Voltage of C2/V | Efficiency |
|----------------------------------|--------------------|--------|-------------------------------|-----------------|------------|
| Silicon Steel sheet (20JNEH1200) | Axially_laminated | 306 | 10.52 | 274 | 8.51% |
| | Radially_laminated | 305 | 11.79 | 446 | 10.73% |
| Iron-cobalt alloy (1J27) | Solid | 340 | 10.23 | 211 | 8.92% |
| | With 8 slits | 293 | 11.54 | 459 | 9.91% |
| Iron (DT4C) | Solid | 338 | 8.24 | 182 | 5.75% |
| | With 8 slits | 292 | 11.45 | 447 | 9.72% |
| Amorphous alloy sheet (1K101) | Radially_laminated | 275 | 10.34 | 394 | 7.45% |
| | Solid | 352 | 8.57 | 275 | 6.51% |
| Permalloy (1J50) | With 8 slits | 311 | 8.89 | 276 | 6.14% |
| | Solid | 201 | 5.72 | 107 | 1.64% |

results by several simulations, the values of the optimal initial position in this model of different armatures are set between -13mm and -15 mm. The external circuit used in this simulation is shown in Fig. 2. The capacitances of C1 and C2 are 1600 μ F and 25 μ F, respectively. The initial voltage of the capacitor bank is set to 500 V.

3.2. Simulation results analysis

The simulation results are listed in Table 5. From the results, we can find that the radially_laminated silicon steel sheets have the highest efficiency. Ferrite has the lowest efficiency. The axially

laminated structure has a lower efficiency than the radially laminated structure. 1J27 and DT4C cylinder with slits have a higher efficiency than solid structure. But the 1J50 has the opposite phenomenon. Next, we will analyze the influence of each factor on the efficiency from the material properties (electric conductivity and saturation flux density) and structure of the armatures.

3.2.1. Electric conductivity

To analyze the influence of the conductivity of the armature to the force, we simulated and compared the force exerted on the armature by assuming the conductivity of some materials to be zero. The simulation results of forces are shown in Fig. 5. 1J27 with

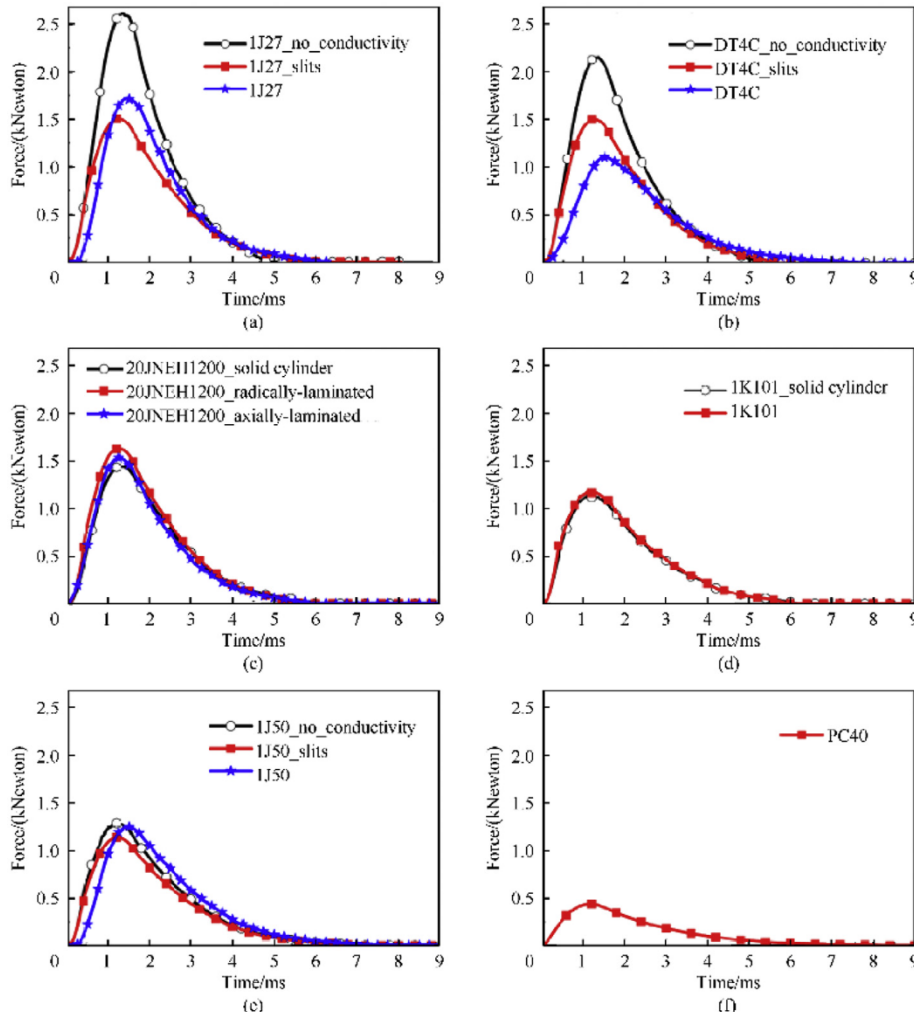


Fig. 5. The forces on the armatures with different structures and different materials.

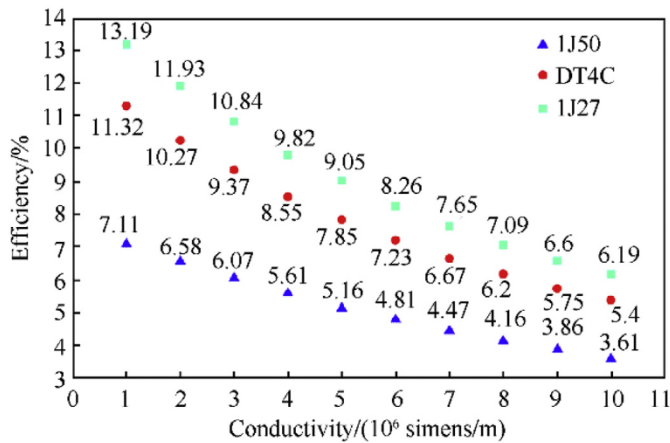


Fig. 6. Simulated efficiencies on different assumed conductivities of 1J50, DT4C, and 1J27.

no conductivity gains a one and a half times larger force than with conductivity. DT4C with no conductivity gains a twice larger force than with conductivity. 1J50 with no conductivity also gains a larger force than with conductivity. Combined with the theory analysis above, these phenomena are caused by the Lorentz force which is generated by eddy current in the conductive armature. According to the theoretical analysis above, higher conductivity will lead to larger eddy current density and greater Lorentz force. Therefore, the conductivity of the material will decrease the resultant force.

After analyzing the influence of conductivity on the force, we continue to study the influence of conductivity on efficiency. We selected three materials of 1J50, DT4C, and 1J27.10 values are uniformly taken between 10^6 Simens/m and 10^7 Simens/m as the hypothetical conductivity, and are simulated by using our model. The simulation results are shown in Fig. 6. It can be seen that the efficiency increases with the decrease of conductivity, and the efficiency will increase about 7%–10% if the conductivity decreases 10^6 Simens/m. When the conductivity is 10^6 Simens/m, the efficiency of 1J27 will reach to 13.19% which is twice when its conductivity is 10^7 Simens/m. The other two materials have the same phenomenon.

3.2.2. Saturation flux density

In order to analyze the effect of the saturation flux density to the efficiency, three sets of data is simulated assuming these materials are with the same conductivities which are 10^6 Simens/m, 5×10^6 Simens/m, and 10^7 Simens/m. The efficiencies of these six kinds of materials are shown in Fig. 7. The order of efficiency from low to high is consistent with the order of saturation flux density. The increase in B_s has a significant effect on the improvement of efficiency. Take the two materials with the most significant B_s difference for example, the saturation flux density of 1J27 is 1.85 T larger than that of PC40, and its efficiency is increased by more than 6 times.

According to the Professor Slade's research [48].

$$m_a \frac{dv_z}{dt} - \pi a^2 \left(\frac{B_{sat} B_z}{\mu_0} - \frac{B_{sat}^2}{2\mu_0} \right) = 0 \quad (36)$$

where a is the radius of the armature, B_z is magnetic flux density in Z-direction, B_{sat} is the saturation flux density of the armature. The force will only depend on the saturation flux density, when the armature is saturated. The armature will spend most of its time in saturated state because of the high magnetic field strength generated by the driving current. It can be seen from Fig. 5, due to the

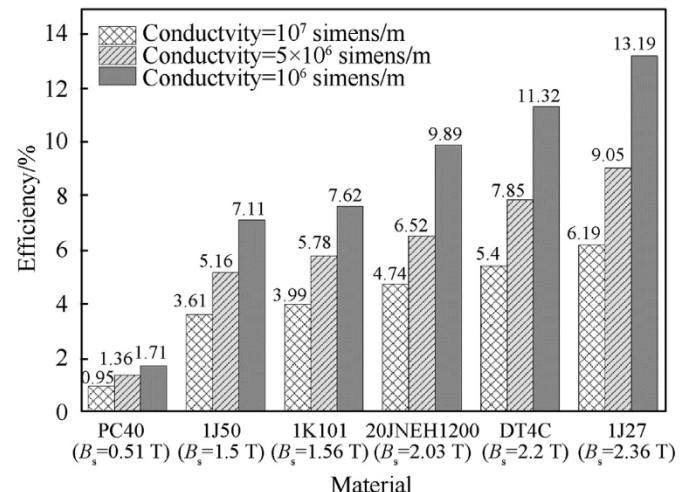


Fig. 7. The efficiencies of different materials with three same assumed conductivity value.

lowest saturation flux density, the ferrite armature gains the smallest force despite owing the lowest conductivity. Hence, saturation flux density is an important index to choose the material of the armature. It can be seen from Figs. 4 and 5, the magnetic permeability has little influence in the efficiency, because the reluctance accelerator spends very short time in low current during the whole launching process.

3.2.3. Structure

In practical application, high saturation flux density and low conductivity cannot be satisfied at the same time in one kind of material, so it is necessary to take some structural measures for the armature to decrease the eddy current density.

Slitting in the armature is one of the methods to restrain the eddy current. The 1J27, DT4C, and 1J50 armatures were all cut by eight slits, and the eddy current densities of armatures sections with two different structures are shown in Fig. 8. It can be seen from Fig. 8 that slitting can indeed cut off the flow of eddy current and reduce the current densities efficiently. According to the force analysis, the Lorentz force can be restrained and the efficiency can be improved. However, according to the relationship between magnetization force and magnetizing volume, the magnetization volume will be lost by slitting. When the Lorentz force is reduced, the magnetization force will be reduced simultaneously. Therefore, 1J27 with the highest magnetic saturation strength does not achieve the highest efficiency after slitting. On the contrary, 1J50 with slits achieves a lower efficiency than solid cylinder.

Therefore, slitting is one of the effective methods to reduce the eddy current density. For materials with high conductivity, slitting is also one of the effective methods to improve the efficiency, e. g 1J27 and DT4C. However, for materials with lower conductivity, slitting may reduce the resultant force and efficiency due to the lost of magnetizing volume, e. g 1J50.

Laminating the ferromagnetic sheets is another effective method to restrain the eddy current. From Fig. 5(c) and (d), it can be seen that the lamination structure gains larger force than the solid structure. The solid structures in Fig. 5(c) and (d) are postulated. The axial lamination is beneficial to reduce the eddy current density due to the insulating layer between silicon steel sheets, but it is not particularly effective compared with the radial lamination. Because the magnetic flux density in the rolling direction of silicon steel sheet is stronger than other directions, and the eddy current

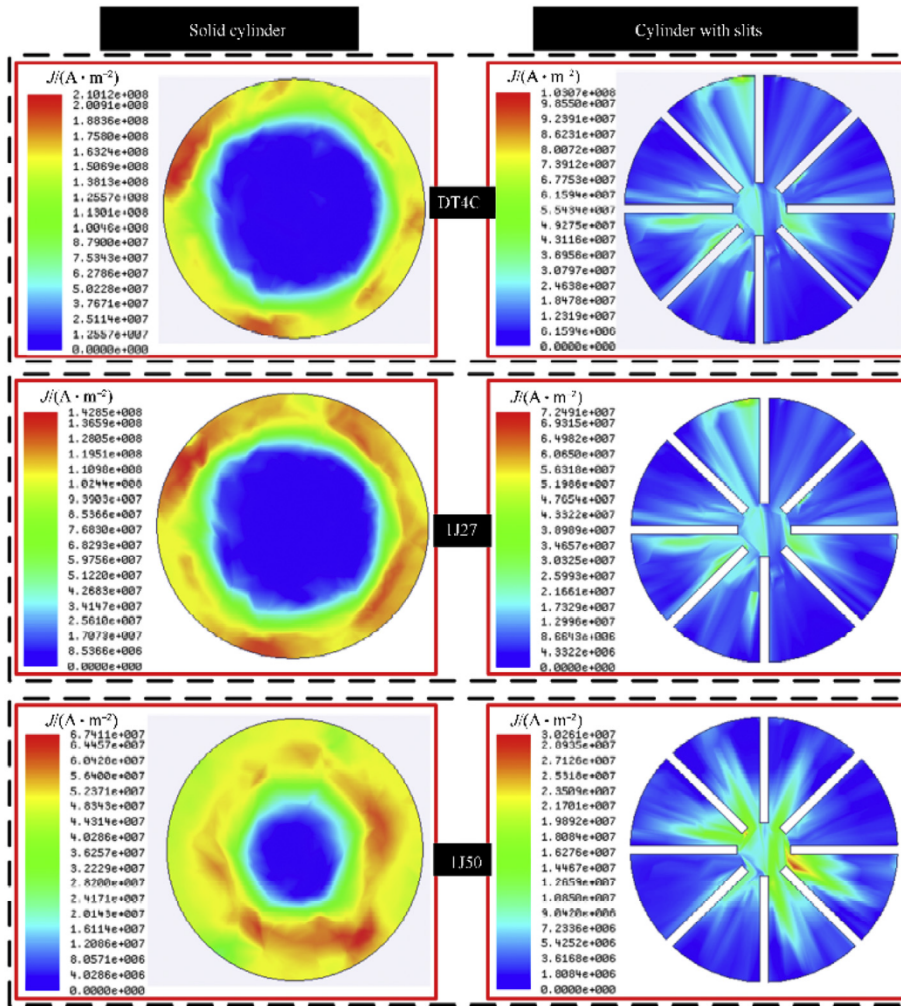


Fig. 8. Eddy current density (J) of armatures sections with two different structures of DT4C, 1J27, and 1J50. (time = 0.5 ms, position = 5 mm from the top surface of the armature).

still exist circumferentially as the sheets to be laminated axially, radial lamination is a better structure compared with the axial lamination.

In summary, slitting and laminating are both effective methods to reduce the eddy current. The negative effect of Lorentz force can be minimized by lamination without wasting too much magnetizing volume. Therefore, the material that has ideal saturation flux density and can be made into laminated structure is an ideal option for armature of reluctance accelerator.

4. Experimental research

4.1. Experimental platform construction

The experimental equipment in this paper is composed of a launcher, pulsed power supply, switches, control system, sensor, velocity-measuring system, data acquisition and processing system. The layout of the experimental equipment is shown in Fig. 9. The launcher consists of an armature, a former, a drive coil. The cylindrical armatures used in the experiment are shown in Fig. 10. The materials and structures are described in Tables 3 and 4. The edge cutting of laminations and slitting of armatures are machined by wire cutting technology. The driving coil is winded with 1.5-mm enameled copper wires on the skeleton made of nylon. A cylindrical hollow was dug in the nylon skeleton, which provides the motion

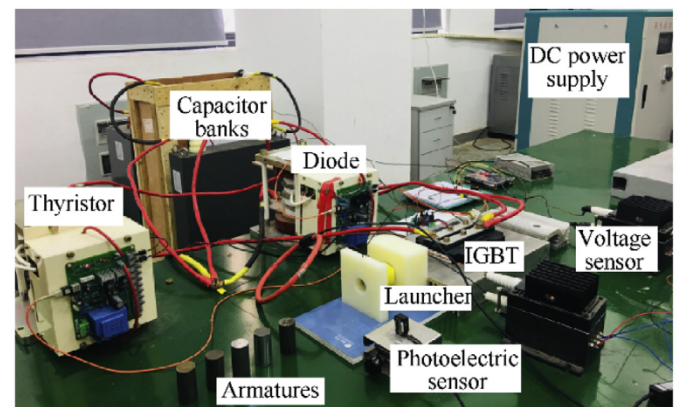


Fig. 9. Experimental layout of the reluctance accelerator.

track for the armature.

The dimensions of the drive coil and the armature are shown in Table 2. The inductance and resistance value of the drive coil are measured by LCR meter. The inductance and resistance value are 403.58 μ H and 228.94 m Ω . In this experiment, the charging voltages for the capacitor bank are set as 500 V. The discharging capacitance and reversed charging capacitor are 1600 μ F and 25 μ F.

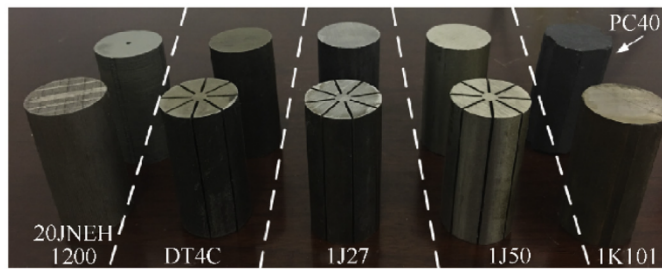


Fig. 10. Different armatures with various materials and structures.

The selected capacitor and voltage are all based on our existing experimental condition.

4.2. Experimental results analysis

The turn off time of IGBT is determined by the time for the armature to reach the middle point of drive coil, thus the armature will gain the best performance. For different armatures, the time to reach the middle of the coil is different. The simulation and experimental curves of currents with different armatures are shown in Fig. 11. Good agreement between the experiment and the simulation is both observed in Fig. 11. The experimental results of different armatures are shown in Table 6, which is in good agreement with simulation results. Experiment reveals the same phenomena as simulation, so it can draw the same conclusions as simulation described above. This demonstrates that the theory and simulation analysis is correct and the design is reasonable.

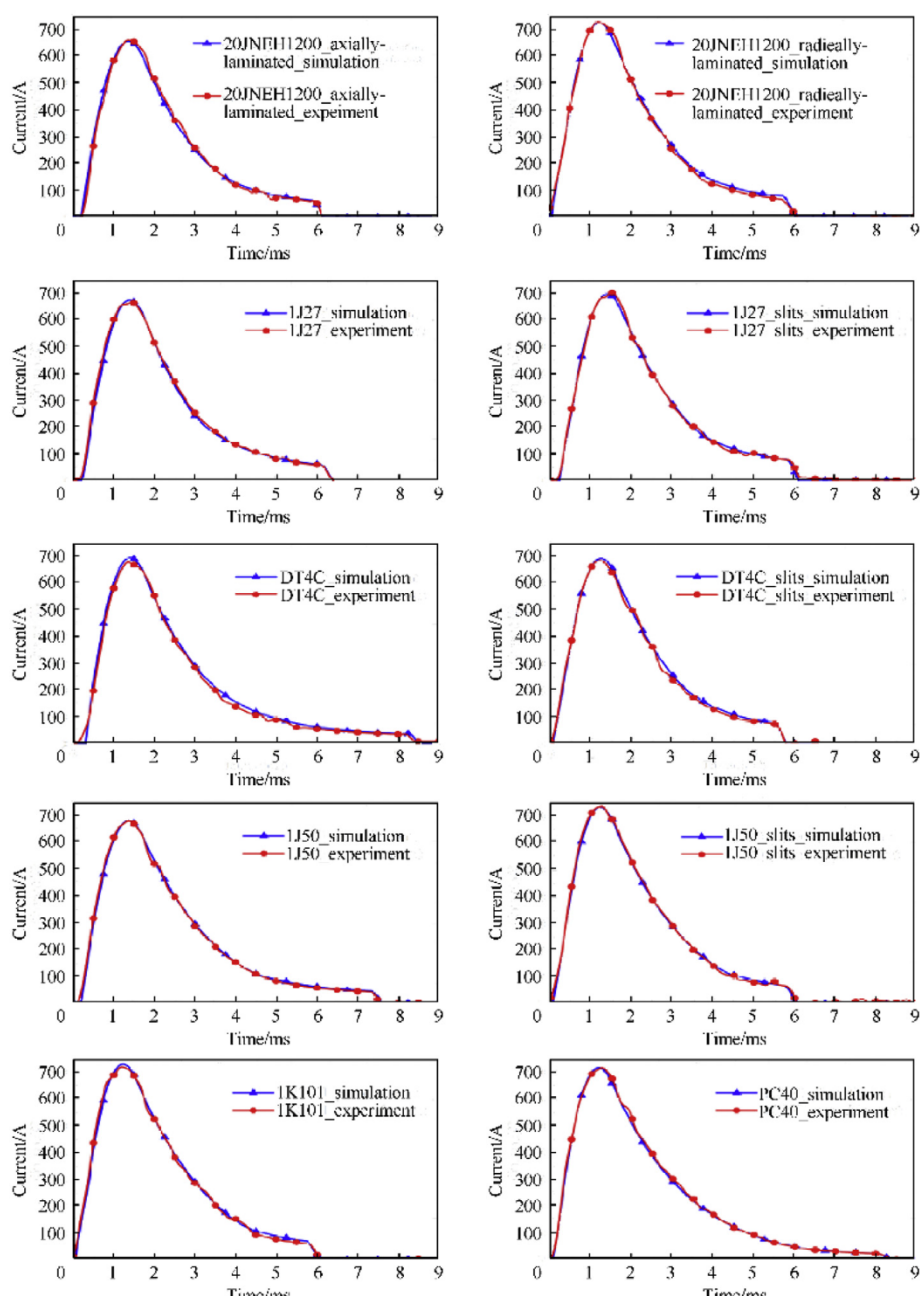


Fig. 11. Simulation and Experimental currents in drive coil by using different armatures.

Table 6

Experimental results of different Armatures.

| Material | Structure | Mass/g | Velocity/(m·s ⁻¹) | Voltage of C2/V | Efficiency |
|-------------------------------|---------------------|--------|-------------------------------|-----------------|------------|
| Silicon | Axially_laminated | 306 | 10.41 | 268 | 8.33% |
| Steel sheet (20JNEH1200) | Radically_laminated | 305 | 11.72 | 442 | 10.62% |
| Iron-colbat alloy (1J27) | Solid | 340 | 10.15 | 208 | 8.79% |
| | With 8 slits | 293 | 11.38 | 453 | 9.61% |
| Iron (DT4C) | Solid | 338 | 8.24 | 176 | 5.75% |
| | With 8 slits | 292 | 11.37 | 445 | 9.50% |
| Amorphous alloy sheet (1K101) | Radically_laminated | 275 | 10.31 | 387 | 7.36% |
| Permalloy (1J50) | Solid | 352 | 8.49 | 270 | 6.37% |
| | With 8 slits | 311 | 8.80 | 272 | 6.07% |
| Ferrite (PC40) | Solid | 201 | 5.62 | 105 | 1.59% |

5. Conclusion

According to the theory, simulation, and experimental analysis, the conductivity of the armature, the saturation flux density and its structure design are all the factors that affect the efficiency of the reluctance accelerator. The saturation flux density is the most important factor, and the conductivity will generate negative force to decrease the efficiency. Although slitting can reduce the Lorentz force, it cannot completely eliminate the induced eddy current, and the slitting will decrease the magnetizing volume and the force surface area. The armature made out of radially-laminated silicon steel sheet with high saturation flux density is the most suitable material and structure for the reluctance armature in this research. Its efficiency reaches to 10.62% in the experiment and is higher than that in previous researches [7,12–16]. It can be concluded that the high saturation flux density is the necessary requirement to choose the armature material. Meanwhile, laminating method is more efficient to restrain the eddy current to improve the efficiency compared with the slitting one.

With the development of science technology, materials with higher saturation flux density and low conductivity may appear in the future, which will simply the fabrication of the armature and improve the efficiency of the reluctance accelerator. Even so, the methods used here and conclusion drawn in this paper also provide a reference for the design of the device that needs electromagnetic force.

Declaration of competing interest

The authors declare that they have no known competing financial interests or personal relationships that could have appeared to influence the work reported in this paper.

Acknowledgement

This work was supported in part by the Fundamental Research Funds for the Central Universities, China [grant number 2682020GF03] and in part by the Foundation of Key Laboratory of Magnetic Suspension Technology and Maglev Vehicle, Ministry of Education, China.

References

- [1] Kolm H, Mongeau P. Basic principles of coaxial launch technology. *IEEE Trans Magn* Mar 1984;20(2):227–30.
- [2] Kim Jihun, Ahn Jaemyung. Modeling and optimization of a reluctance accelerator using DOE-based response surface methodology. *J Mech Sci Technol* 2017;31(3):1321–30.
- [3] Orbach Yaft, Oren Matan, Golan Aviv, Einat Moshe. Reluctance launcher coilgun simulations and experiments. *IEEE Trans Plasma Sci* 2019;47(2):1358–63.
- [4] Bresie DA, Andrews JA. Design of a reluctance accelerator. *IEEE Trans Magn* 1991;41(11):623–7.
- [5] Mark H. Electromagnetic launch technology: the promise and the problems. *IEEE Trans Magn* 1989;25(1):17–9.
- [6] El-Hasan Tareq S. Design of a single stage supersonic reluctance coilgun (RCG). In: IEEE pulsed power conference; Apr. 2012; 2011.
- [7] Slade GW. A simple unified physical model for a reluctance accelerator. *IEEE Trans Magn* 2005;41(11):4270–6.
- [8] Laithwaite ER. A history of linear electric motors. London, U.K.: Macmillan; 1987.
- [9] Mendrela EA, Pudlowski ZJ. Transients and dynamics in a linear reluctance self-oscillating motor. *IEEE Trans Energy Convers* 1992;7(1):183–91.
- [10] Rizzo M. A linear reluctance self-oscillating motor. *Transactions on the Built Environment* 1995;12:193–200.
- [11] Rivas-Camacho JL, Ponce-Silva M, Olivares-Peregrino VH. The ringer as an inductive power source for a reluctance accelerator. *IEEE Trans Plasma Sci* 2019;47(5):2275–81.
- [12] Barrera T, Beard R. Exploration and verification analysis of a linear reluctance accelerator. In: 17th IEEE international symposium on electromagnetic launch technology (EML), Jul 07–11; 2014.
- [13] Daldaban F, Sari V. Design and implementation of a three-coil linear reluctance launcher. In: 16th international power electronics and motion control conference and exposition, Sep 21–24; 2014.
- [14] Xiang Hongjun, Lei Bin, Li Zhiyuan, Zhao Keyi. Design and experiment of reluctance electromagnetic launcher with new-style armature. *IEEE Trans Plasma Sci* 2013;41(5):1066–9.
- [15] Hou Yanpan, Liu Zhenxiang, Ouyang Jian-Ming, Dong Yang. Parameter settings of the projectile of the coil electromagnetic launcher. In: 16th international symposium on electromagnetic launch technology, may 15–19; 2012.
- [16] Daldaban F, Sari V. The optimization of a projectile from a three-coil reluctance launcher. *Turk J Electr Eng Comput Sci* 2016;24(4):2771–88.
- [17] Deng Huimin, Wang Yu, Lu Falong, Yan Zhongming. Optimization of reluctance accelerator efficiency by an improved discharging circuit. *Defence Technology* 2020;16(3):662–7.
- [18] William Slade G. Fast finite-element solver for a reluctance mass accelerator. *IEEE Trans Magn* 2006;42(9):2184–92.
- [19] Mosallanejad A, Shoulaie A. A novel structure to enhance magnetic force and velocity in tubular linear reluctance motor. *Turk J Electr Eng Comput Sci* 2012;20:1063–76.
- [20] Zhao Keyi, Xiang Hongjun, Li Zhiyuan, Lei Bin, Zhang Qian, Song Liwei, Li Jinming. Optimum design of driving circuit parameters for magnetic-resistance coil launcher. In: 17th IEEE international symposium on electromagnetic launch technology (EML), jul 07–11; 2014.
- [21] Perotoni MB, Mergl M, Bernardes VA. Coilgun velocity optimization with current switch circuit. *IEEE Trans Plasma Sci* 2017;45(6):1015–9.
- [22] Cooper Liam M, Van Cleef Abigail R, Bristoll Bernard T, Bartlett Paul A. Reluctance accelerator efficiency optimization via pulse shaping. *IEEE Access* 2014;2:1143–8.
- [23] Harris Michael J, Maher Shaikh, Bristoll BT, Vine K, Bartlett Paul A. The efficiency of a two-stage reluctance accelerator through pulse shaping. *IEEE Access* 2016;5:121–7.
- [24] Reza M, Iqbal SJ, Hon KW. Better performance pulsed launcher system by adjusting projectile initial position. In: 2nd IEEE international conference on power and energy (PECon 08), December; 2008. p. 1–3.
- [25] Rivas-Camacho Luis, Ponce-Silva Jorge, Mario Olivares-Peregrino, Victor H. Experimental results concerning to the effects of the initial position of the projectile on the conversion efficiency of a reluctance accelerator. In: 13th international conference on power electronics (CIEP), Jun 20–23; 2016.
- [26] Slade William. Notes on the effects of metallic coil sheaths and armature losses in reluctance coilguns. <http://users.skynet.be/BillsPage/SimulationResults1.0.pdf>.
- [27] Tandon SC, Armor AF, Chari MVK. Nonlinear transient finite element field computation for electrical machines and devices. *IEEE Trans Power Apparatus Syst* 1983;102(5):1089–96. PAS.
- [28] Isfani Basim F. Extensions to the finite element method for nonlinear magnetic field problems. Rensselaer Polytechnic Institute Ph.D. Thesis; 1987.
- [29] Pechstein Clemens, Jüttler Bert. Monotonicity-preserving interproximation of B-H-curves. *J Comput Appl Math* 2006;196(1):45–57.

- [30] Akima Hiroshi. A new method of interpolation and smooth curve fitting based on local procedures. *J ACM* 1970;17(4):589–602.
- [31] Bica AM. Optimizing at the end-points the Akima's interpolation method of smooth curve fitting. *Comput Aided Geomet Des* 2014;31(5):245–57.
- [32] Carpenter CJ. Surface-integral methods of calculating forces on magnetized iron parts. *Proc IEEE Part C: Monographs* 1960;107(11):19–28.
- [33] Carter GW. Distribution of mechanical forces in magnetised material. *Proc Inst Electr Eng* 1965;112(9):1771–7.
- [34] Aldefeld B. Numerical calculation of electromagnetic actuators. *Electr Eng* 1979;61(6):347–52.
- [35] Jacobus A, Muller W. Numerical solution of forces and torques. *IEEE Trans Magn* 1983;19(6):2589–92.
- [36] Demerdash NA, Mohammed OA, Nehl TW. Forces on conductor segments and magnetized ferrous cores using a three dimensional finite element vector potential method. *IEEE Trans Energy Convers* 1986;1(3):109–17. EC.
- [37] Reyne G, Sabonnadiere J, Coulomb J, et al. A survey of the main aspects of magnetic forces and mechanical behaviour of ferromagnetic materials under magnetization. *IEEE Trans Magn* 1987;23(5):3765–7.
- [38] Wignall AN, Gilbert AJ, Yang SJ. Calculation of forces on magnetised ferrous cores using the Maxwell stress method. *IEEE Trans Magn* 1988;24(1):459–62.
- [39] Muller W. Comparison of different methods of force calculation. *IEEE Trans Magn* 1990;26(2):1058–61.
- [40] Ren Z. Comparison of different force calculation methods in 3D finite element modelling. *IEEE Trans Magn* 1994;30(5):3471–4.
- [41] Cai W, Pillay P, Reichert K. Accurate computation of electromagnetic forces in switched reluctance motors. *Proceedings of the Fifth International Conference on Electrical Machines and Systems* 2001.
- [42] Lee SH, He X, Kim DK, et al. Evaluation of the mechanical deformation in incompressible linear and nonlinear magnetic materials using various electromagnetic force density methods. *J Appl Phys* 2005;97(10). 10E108-1-3.
- [43] Lee SH, Han SJ, Choi HS, et al. Magnetic force distributions in saturated magnetic system using magnetic charge method and other methods. *IEEE Trans Appl Supercond* 2004;14(2):682–5.
- [44] Zahn Markus. Derivation of the Korteweg-Helmholtz electric and magnetic force densities including electrostriction and magnetostriction from the quasistatic Poynting's theorems. In: *IEEE conference on electrical insulation & dielectric phenomena*, oct 15–18; 2006.
- [45] Henneberger G, Sattler PK, Shen D. Nature of the equivalent magnetizing current for the force calculation. *IEEE Trans Magn* 1992;28(2):1068–71.
- [46] Kabashima T, Kawahara A. Force calculation using magnetizing currents. *IEEE Trans Magn* 1988;24(1):451–4.
- [47] Coulomb J. A methodology for the determination of global electromechanical quantities from a finite element analysis and its application to the evaluation of magnetic forces, torques and stiffness. *IEEE Trans Magn* 1983;19(6):2514–9.
- [48] Slade William. A brief theoretical study of reluctance-based mass accelerators and actuators. <http://users.skynet.be/BillsPage/MassAccel1.pdf>.